Stability of simple cubic calcium at high pressure: A first-principles study

Yansun Yao,[1] Roman Martoňák,[2] Serguei Patchkovskii,[1] and Dennis D. Klug[1]
[1]*Steacie Institute for Molecular Sciences, National Research Council of Canada, Ottawa, Canada K1A 0R6*
[2]*Department of Experimental Physics, Comenius University, Mlynská dolina F2, 842 48 Bratislava, Slovakia*
(Received 17 March 2010; revised manuscript received 13 May 2010; published 14 September 2010)

The origin of the temperature dependence of the stability of the simple cubic (sc) structure of Ca in the pressure range 32–109 GPa is investigated by the use of plane-wave density-functional calculations and first-principles molecular-dynamics (MD) simulations based on localized basis set method employed in the SIESTA code. Constant-pressure MD simulations are performed on the competing sc and $I4_1/amd$ structures in this pressure range. The results are analyzed to recover details of the structures and dynamics at 300 K of sc and the recently predicted 0 K lowest-enthalpy $I4_1/amd$ structure of Ca. The structure at 300 K appears to be an almost pure sc structure and not an average of sc and the lowest enthalpy $I4_1/amd$ structure. The stability of the $I4_1/amd$ structure at 0 K is suggested to partially result from differences in Coulombic core interactions. The enthalpy difference between $I4_1/amd$ and sc is much less at 300 K than at 0 K also indicates that the sc structure is becoming more stable with increasing temperature.

DOI: 10.1103/PhysRevB.82.094107 PACS number(s): 61.66.Bi, 61.50.Ks, 63.20.D−, 74.70.−b

I. INTRODUCTION

Recent experiments on elemental Ca described a series of phase transitions under high pressure with several crystal structures identified.[1–3] The high-pressure phase transitions of Ca feature a decreasing of packing efficiency of atoms at pressures less than 109 GPa, which contrasts with the intuitive expectation that the crystal structures would become more closed packed upon compression. This special behavior was investigated recently, and it is now accepted that it is induced by a continuous lowering and filling of the initially unoccupied *d* bands.[4] At ambient pressure Ca crystallizes in a face-centered-cubic (fcc, Ca-I) structure. Olijnyk *et al.*[5] reported that Ca transforms to a body-centered cubic (bcc, Ca-II) at 20 GPa and then to a simple cubic (sc, Ca-III) at 32 GPa. The sc structure remains stable up to 109 GPa and further transforms to two new phases, Ca-IV at 113 GPa and Ca-V at 139 GPa.[2] Ishikawa *et al.*[6] initially predicted that Ca-IV and Ca-V have $P4_32_12$ and *Cmca* symmetry by metadynamics[7] and molecular-dynamics (MD) simulations. Using a different approach, Yao *et al.*[8] predicted the same *Cmca* structure for Ca-V but a different structure for Ca-IV with a *Pnma* space group. Recently Fujihisa *et al.*[1] were able to fit the experimental x-ray diffraction (XRD) patterns of Ca-IV and Ca-V into the $P4_32_12$ and *Cmca* structures, although other possible fittings may exist. On the other hand, since the *Pnma* structure is more energetically favorable than Ca-V at higher pressure, it might be a new phase (Ca-VI). This was suggested in a recent study by Ishikawa *et al.*[9] and confirmed by experiment by Nakamoto *et al.*[10] Another post Ca-V model is the incommensurate $I4/mcm(00\gamma)$ structure proposed by Arapan *et al.*[11] based on analogies with similar elements. While Ca-IV and Ca-V have attracted significant attention, the precise structure of lower-pressure Ca-III has not been fully resolved, and debates were initiated recently.

The structure of Ca-III was studied by several different groups using XRD methods. In all experiments, sc was the only observed structure [see, e.g., Olijnyk *et al.* (1984),[5] Yabuuchi *et al.*(2005),[2] Fujihisa *et al.*(2008),[1] and Gu *et al.*(2009) (Ref. 3)]. However, density-functional theory (DFT) calculations showed that the sc structure is a mechanically unstable phase for Ca (Refs. 12–14) [see, e.g., Gao *et al.* (2008), Teweldeberhan *et al.* (2008), and Errea *et al.* (2008)]. There were different interpretations for this inconsistency. Since the experiments were performed at finite temperature but the DFT calculations essentially describe the ground states at 0 K, one intuitively expects that the temperature effects would play an important role. By studying the unstable vibrational modes of sc, Teweldeberhan *et al.*[13] derived a lower symmetry *Cmcm* for Ca-III, and furthermore, explicitly excluded sc from the phase diagram. Errea *et al.*,[14] on the other hand, suggested that sc is a stable phase and attributed its stability to anharmonic effects enhanced by temperature. The latter interpretation is supported by a recent study by Yao *et al.*,[15] where the sc structure is identified for Ca-III at room temperature using metadynamics simulations. Moreover, Yao *et al.*[15] and Oganov *et al.*[16] also predicted the existence of a lower enthalpy $I4_1/amd$ phase at low temperature. Very recently, Yin *et al.*[17] provided another interpretation along this line. They assumed that since the proposed models are energetically and structurally very close to sc, the observed "sc" phase could be interpreted as a highly anharmonic phase derived from a spatially inhomogeneous and dynamically fluctuating combination of multiple structures. In other words, the experimentally observed sc structure is an average of several structures. Although all these studies shed light towards a more complete understanding, these interpretations still have apparent contradictions. The contradictions, in fact, all originate from one fundamental point, that is whether sc is indeed the true stable phase at room temperature as indicated by experiments. Should, for example, the experimental XRD pattern be unambiguously interpreted as a sc structure, not an average structure, or even a different phase? If sc is stable at room temperature, how does it overcome the fairly significant energy difference from the ground state $I4_1/amd$ phase? If it is unstable, can it collapse to another phase, or just fluctuate between competing structures? The answers to these questions are essential to solve this puzzle and motivated the present study. In the present study,

we extensively investigated the thermal stability of sc structure from the following approaches. (1) We performed a microscopic study of the electronic structure and static stability for sc structure using the DFT method, and provided a rationalization for its instability at 0 K. (2) We performed first-principles MD simulations to investigate the thermal stability for the sc structure at room temperature. We provided a quantitative analysis of the thermal trajectories and derived the structure factors, in an effort to interpret the experimental XRD pattern and characterize its structural stability. We also calculated the enthalpies and characterized the energetics for the sc structure at room temperature. In all these analyses, the properties of sc are compared with those of the lowest enthalpy $I4_1/amd$ structure, which serves as a benchmark. We obtain conclusions from these analyses and provide a discussion connecting the present and previous studies.

II. METHODS

A. Theory

At 0 K and pressure P, the stability order of competing structures are determined by their enthalpy H,

$$H = E_0 + PV. \tag{1}$$

Here E_0 is the static crystal energy of the system with interacting electrons and nuclei (cores). At 0 K, a complete description of the energetics also includes the contributions from lattice vibrations or zero-point energy. Since the sc structure has imaginary phonon modes at 0 K, the zero-point energy cannot be calculated within the harmonic approximation and therefore, is omitted in Eq. (1). The motions of electrons and nuclei are separated, therefore,

$$E_0 = E_{electron} + E_{core}. \tag{2}$$

Here E_{core} accounts for the direct Coulombic interactions between the nuclei (Ewald summations[18,19]). $E_{electron}$ is the total electronic energy,

$$E_{electron} = E_{kin} + E_{ec} + E_H + E_{\mathrm{xc}}, \tag{3}$$

which includes the electronic kinetic energy E_{kin}, electron-nucleus interaction energy E_{ec}, electron-electron Coulomb energy E_H (Hartree term), and electronic exchange-correlation (xc) energy E_{xc}.

In the present study, E_{core} and $E_{electron}$ were calculated using the pseudopotential approach within the Kohn-Sham (KS) formalism[20] of DFT. Since the effects of core electrons are included in the pseudopotential, the terms E_{core} and $E_{electron}$ used in this study refer to the energies of pseudocores and valence electrons. In the KS formalism of DFT, $E_{electron}$ is derived from the summation of quasiparticle eigenvalues of occupied states,

$$E_{electron} = \sum_i \varepsilon_i - E_H + \Delta E_{\mathrm{xc}}. \tag{4}$$

Here ε_i represents the eigenvalue at state i. Since KS formalism of DFT maps the interacting many-electron system onto a system of many noninteracting quasiparticles, the sum of quasiparticle eigenvalues does not directly give $E_{electron}$ because it double counts the Hartree energy and miscounts the xc energy. Thus, in Eq. (4), a Hartree term E_H has been subtracted and a correction to xc energy ΔE_{xc} has been added.

When the temperature T is above 0 K, the stability order of competing structures at pressure P is determined by their Gibbs free energies. In addition to the enthalpy, the Gibbs free energy also includes the vibrational free energy F_{vib} and electronic entropy $S_{electron}$ that are functions of temperature. Due to thermal expansion, E_0 and PV will also change with temperature. $S_{electron}$ can be approximated from the Fermi distribution of noninteracting electrons with the energy distribution described by electronic density of states (eDOS). Since only electrons within a narrow shell of k_BT around the Fermi level contribute to the excitation, the electronic entropy is usually very small and has negligible contribution to the structural stability. The vibrational entropy S_{vib} has two contributions, one from the harmonic part of vibrational density of states (vDOS) that is unchanged with temperature, and the other from the anharmonic part of vDOS that is temperature dependent. If the anharmonicity is not excessively large in the system, the S_{vib} can be reasonably estimated from the quasiharmonic approximation (QHA) using the Bose-Einstein distribution of noninteracting quantized lattice oscillations (phonons) with the frequency distribution described by vDOS. In QHA, anharmonic effects are accounted for by allowing phonon frequencies to depend only on crystal volume.[21] In a MD simulation where anharmonicity is explicitly included, the vDOS is the normalized Fourier transform of the single-particle velocity autocorrelation function,[22]

$$g_T(\omega) = \int e^{-i\omega t}\langle \vec{v}_T(t) \cdot \vec{v}_T(0)\rangle dt. \tag{5}$$

Here $g_T(\omega)$ is the vDOS evaluated at temperature T. $\vec{v}_T(0)$ and $\vec{v}_T(t)$ are the atomic velocities at the time origin and at a time t later. The bracket denotes an ensemble average over all atoms in the system.

The structural changes during the MD simulations employed in the present study were monitored by calculation of the structure factors.[23] The instantaneous structure factor at time t is

$$S(\vec{q},t) = \frac{1}{N}|\rho(\vec{q},t)|^2, \tag{6}$$

where N is the number of atoms in the system and the density operator $\rho(\vec{q},t)$ is defined as

$$\rho(\vec{q},t) = \sum_{i=1}^{N} b_i(\vec{q})\exp[-i\vec{q}\cdot\vec{r}_i(t)]. \tag{7}$$

Here $\vec{r}_i(t)$ is the instantaneous position for atom i at time t. For x-ray diffraction, $b_i(\vec{q})$ is the atomic scattering form factor for atom i at wave vector $\vec{q}$. $\vec{q}$ represents the momentum transferred during scattering, and is related to the scattering angle 2θ and wavelength λ of incoming radiation by

$$|\vec{q}| = \frac{4\pi \sin\theta}{\lambda}. \quad (8)$$

The static structure factor $S_s(\vec{q})$ is a time average of the instantaneous structure factor $S(\vec{q},t)$,

$$S_s(\vec{q}) = \frac{1}{N}\langle|\rho(\vec{q},t)|^2\rangle_t. \quad (9)$$

The coherent part of $S_s(\vec{q})$ accounts for the contribution from Bragg scattering per atom,

$$S_c(\vec{q}) = \frac{1}{N}|\langle\rho(\vec{q},t)\rangle_t|^2. \quad (10)$$

The difference between $S_s(\vec{q})$ and $S_c(\vec{q})$ represents the diffuse scattering. The peaks for $S_c(\vec{q})$ at specific values of $\vec{q}$ correspond to the Bragg reflections observed in a diffraction experiment at wavelength λ. A change in the positions of Bragg peaks indicates a change in interplanar spacing (d_{hkl}) of the lattice, and usually corresponds to a phase transition. $S_s(\vec{q})$ also contains the diffuse contribution, which captures the information on the dynamical disorder of the system arising from thermal vibrations and static disorder.

B. Computational details

Structural optimizations, enthalpies, and *e*DOS were calculated for sc, bcc, and $I4_1/amd$ structures using two different first-principles implementations of DFT. The first implementation employed a localized basis set for wave-function expansion with the SIESTA method.[24] The second implementation used a plane-wave basis set for wave functions with projected augmented wave (PAW) corrections.[25] The two types of calculations were performed using SIESTA and VASP (Ref. 26) codes, along with norm-conserving and PAW pseudopotentials, respectively. Both pseudopotentials contain semicore states 3*s* and 3*p* in the valence, and employed the Perdew-Burke-Ernzerhof xc functional.[27] The plane-wave basis set was expanded with a maximum kinetic energy of 350 eV. The localized basis set consisted of a double-ζ basis with two polarization radial functions for 4*s* and 3*d* states, and a single-ζ basis with one radial function for 3*s*, 3*p*, and 4*p* states. It has proven necessary to improve the flexibility of radial part of the 3*d* basis functions of the standard SIESTA semicore double-ζ basis set for Ca. The additional radial function uses soft cut-off radius of 4.90 bohr. All the remaining basis functions remain identical to the standard basis, optimized for cubic $CaTiO_3$.[28] In the SIESTA method, the electron density is calculated using an auxiliary basis set with a uniform real-space grid defined by an energy cutoff of 250 Ry. The Brillouin-zone (BZ) integrations were performed with a $16\times16\times16$ Monkhorst-Pack mesh.[29] Electron localization functions[30] (ELFs) were calculated at selected pressures using the VASP code, with real-space grids $120\times120\times120$ for sc, and $120\times120\times60$ for $I4_1/amd$ structures, respectively. First-principles MD simulations were performed for sc and $I4_1/amd$ structures using the SIESTA code, with the pseudopotential and basis set described above. The calculations employed an isothermal-isobaric

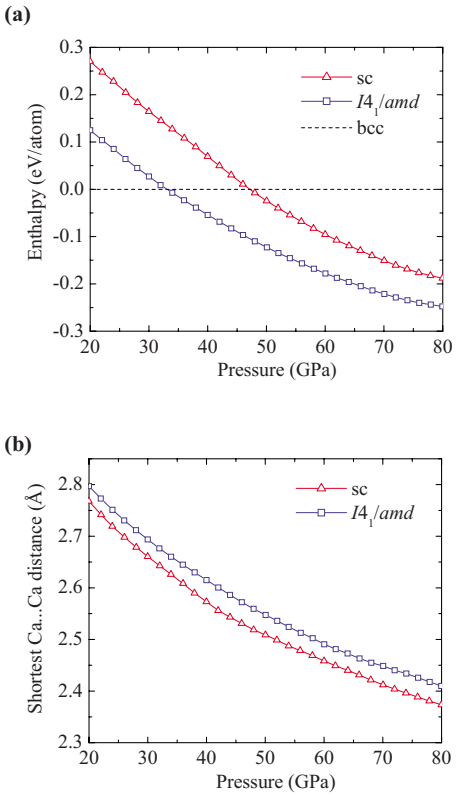

FIG. 1. (Color online) Calculated pressure dependence of (a) enthalpies relative to the bcc structure and (b) shortest Ca···Ca distances of sc and $I4_1/amd$ structures at 0 K.

(*NPT*) ensemble and a 64-atom supercell for each structure. The *NPT* ensemble closely mimics the experimental conditions with both unit cell and internal coordinates allowed to change to adjust to the external pressure and temperature. The ionic temperature was controlled by a Nosé thermostat[31] while the pressure was controlled by a Parrinello-Rahman barostat.[32] The MD simulations were performed at 300 K and 60 GPa. BZ sampling was restricted to the zone center. For each structure, the MD simulation was carried out for 10 ps after 3 ps equilibration time. MD trajectories were sampled with a 1 fs time interval. $S_s(\vec{q})$, $S_c(\vec{q})$, and $g_T(\omega)$ were calculated using the sampled MD trajectories.

III. RESULTS AND DISCUSSION

The pressures for phase transitions at 0 K are estimated by comparing the enthalpies *H* of competing structures. Figure 1(a) shows the enthalpies of the sc and $I4_1/amd$ structures between 20 and 80 GPa, calculated using localized basis set and SIESTA program. The enthalpy for the bcc structure is taken as a reference. Among these structures, bcc is the most stable phase at low pressure, and transforms to $I4_1/amd$ structure at 33 GPa. The sc structure has lower enthalpy than bcc at pressures higher than 47 GPa but never becomes more stable than the $I4_1/amd$ structure in the studied pressure range. The calculated energy orders and pressures for phase transitions in Fig. 1(a) agree well with the previous enthalpy calculations using plane-wave basis set and the VASP pro-

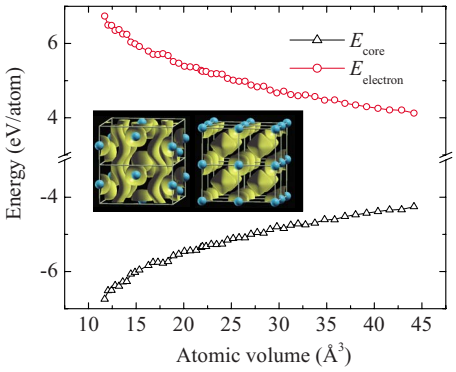

FIG. 2. (Color online) Calculated pressure dependence of E_{core} and $E_{electron}$ of the $I4_1/amd$ structure relative to the sc structure. (Inset) Calculated electron localization function (ELF) for (left) the $I4_1/amd$ and (right) sc structures at 60 GPa with ELF value=0.6.

gram, in which the $I4_1/amd$ and sc structures were found being more stable than bcc at 34 GPa and 41 GPa, respectively.[15] As seen in Fig. 1(a), the enthalpy difference between the $I4_1/amd$ and sc structures is notably large, i.e., −0.14 and −0.076 eV/atom at 20 GPa and 60 GPa, respectively. This suggests that the $I4_1/amd$ structure is stable and may exist at low temperature while the observed sc structure is a metastable phase at room temperature whose stability is most likely facilitated by temperature effects.

Although being significantly more stable at 0 K, the $I4_1/amd$ structure is closely related to sc and can be considered as a distorted form of the latter. The two structures can be connected, for example, via a common *Pmma* subgroup with a fairly small activation barrier.[15] Within the *Pmma* space group, a sc lattice occupies symmetry sites $2e$ $(1/4,\ 0.0,\ 3z)$ and $2f$ $(1/4,\ 1/2,\ z)$ with $z=0$. Once the value of z increases to 1/8, the space group reduces to $I4_1/amd$. The shifts of atoms along z axis result into increase in c/a ratio and volume expanding, and therefore make the $I4_1/amd$ structure less dense than sc. Figure 1(b) shows the calculated shortest Ca···Ca distances in the $I4_1/amd$ and sc structures as a function of pressure. It is clear that the sc structure is always more compact than the $I4_1/amd$ structure at 0 K. At 60 GPa and 0 K, the atomic volume of $I4_1/amd$ structure is about 1.5% larger than that of sc. Moreover, a larger atomic volume for the $I4_1/amd$ structure would tend to destabilize the structure by a greater PV term, but the static crystal energy E_0 has a large drop in the $I4_1/amd$ structure, which mitigates against the destability. At 60 GPa and 0 K, E_0 would drop by 0.16 eV/atom once the sc distorts to $I4_1/amd$ structure. Given that the $I4_1/amd$ structure is only a distorted form of sc, it is interesting to examine why small distortions in structure can result into significant drop in energy.

An instructive way to investigate E_0 and its origin is to separate it into individual contributions from cores E_{core} and electrons $E_{electron}$. The values of E_{core} and $E_{electron}$ were therefore calculated for the sc and $I4_1/amd$ structures and the results are presented in Fig. 2. It is seen that, over the entire pressure range studied, E_{core} favors the $I4_1/amd$ structure and $E_{electron}$ favors the sc structure, while the sum of these two terms favors the $I4_1/amd$ structure. The Coulombic interactions among the cores therefore stabilize the $I4_1/amd$ structure. This observation can be qualitatively explained by the larger atomic volume and longer Ca···Ca distances in the $I4_1/amd$ structure [Fig. 1(b)]. E_{core} results from long-range Coulombic interactions and is determined by the arrangement of cores. The dependence of E_{core} on the atomic volume V is proportional to $V^{-1/3}$, which makes E_{core} favor structures with larger volumes. At 60 GPa and 0 K, the E_{core} in the $I4_1/amd$ structure is −4.9 eV/atom lower than that in the sc structure. $E_{electron}$ takes the opposite trend and competes with E_{core}. The valence electrons in the sc structure are concentrated in the interstitial regions and become more localized than those in the $I4_1/amd$ structure (inset of Fig. 2). As a result of electron localization, E_{kin} will increase, while E_{ec} and E_{xc} will decrease in the sc structure. E_H follows the same trend as E_{core} (as they are both Coulombic terms) and increases in sc structure. At 60 GPa and 0 K, the energy difference between the $I4_1/amd$ and sc structures from E_{kin}, E_{ec}, E_{xc}, and E_H terms are, −1.43, 7.86, 0.29, and −1.98 eV/atoms. The sum of these four terms in the $I4_1/amd$ structure provides a 4.74 eV/atom energy gain in $E_{electron}$, which is less than the energy lost in E_{core} of −4.9 eV/atom, resulting a net energy drop in E_0 of −0.16 eV/atom from the sc structure at 60 GPa. Examples of conditions where E_{core} plays a decisive role in structural stability of competing phases, have also been seen in other pressure-induced phase transitions, for example, diamond to β-Sn transition of Si and Ge.[18,33,34]

At room temperature, the observed pressure-induced transitions in Ca, fcc→bcc→sc, follows a path of decreasing packing efficiency of atoms. This special behavior is the consequence of lowering and filling the initially empty $3d$ bands.[4] With increasing pressure, the $3d$ bands would gradually move below the Fermi level and be filled by the valence electrons that migrate from the $4s$ bands. The occurrence of a $I4_1/amd$ structure, added length to the transition sequence and raises an immediate question, does the appearance of $I4_1/amd$ structure follow the same $s\rightarrow d$ mechanism or is it just an isolated example? This question can be addressed from the investigation of eDOS and its projection to different orbitals. $E_{electron}$ is derived from the occupied eigenvalue sum [Eq. (4)] and therefore depends on the characteristic shape of eDOS. In Fig. 3, the percentages of d electrons in valence bands are presented as functions of pressures for bcc, sc, and $I4_1/amd$ structures. In all three structures, the d component increases with pressure, which is associated with a gradually filling of $3d$ bands. The sc structure always has significantly larger d component than bcc, i.e., more than 10% larger over the entire pressure range. The sc structure also has slightly higher d component than the $I4_1/amd$ structure. As d electrons are critical in stabilizing the electronic structure in Ca, this trend readily indicates that $E_{electron}$ favors sc the most with bcc being the least favored structure. Quantitative calculations confirmed this expectation. The calculated $E_{electron}$ in bcc is 8.87 eV/atoms higher than that of $I4_1/amd$ at 60 GPa, and as described above, the latter is 4.74 eV/atoms higher than that of sc at same pressure. As a response to $E_{electron}$, E_{core} takes the reverse trend and favors bcc the most and sc the least. This suggests that, if there were no $s\rightarrow d$ transition stabilizing the electronic system, the core-

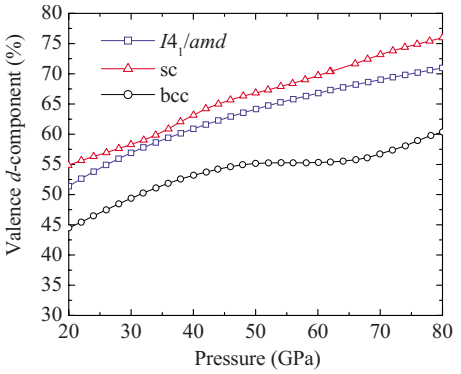

FIG. 3. (Color online) Calculated pressure dependence of the percentages of d electrons in valence bands for the bcc, sc, and $I4_1/amd$ structures.

core repulsion would dominate the phase transitions in Ca and bcc would be the most stable structure at all pressures.[4] The present transition sequence, therefore, results from a balance of competition between the Coulombic interaction of cores and the $s \rightarrow d$ transition of electrons.

Enthalpy calculations [Fig. 1(a)] suggest that the sc structure is not a stable phase of Ca at 0 K and bcc would transform to $I4_1/amd$ structure at sufficient high pressure. In previous experiments,[1–3,5] while all done at room temperature, this phase transition has not been observed. Instead, the bcc structure was found to transform to the sc structure at high pressure. The inconsistency in the predicted transition pathways and observed at different temperatures indicated that, the temperature effects as well as the enhanced anharmonicity, play a critical role in this phase transition and in the (meta)stability of sc structure.[14] To rationalize the temperature effects, first-principles MD simulations were performed for the sc and $I4_1/amd$ structures at 60 GPa and 300 K (room temperature). Within the employed simulation time of 13 ps, no phase transitions were detected in either structure. As seen in Fig. 4(a), the instantaneous values of enthalpy fluctuate due to volume oscillations but the average enthalpies derived from the MD trajectories are almost degenerate for the two structures. The calculated average enthalpies are, −991.1705 and −991.1653 eV/atom for the $I4_1/amd$ and sc structures, respectively. It is notable that at room temperature, the enthalpy difference between the two structures narrows down to about 0.005 eV/atoms, which is only 7% of the value of 0.076 eV/atom calculated at 0 K [Fig. 1(a)]. The sc structure becomes much more energetically favorable and accessible at room temperature than at 0 K. The $I4_1/amd$ structure has larger volume fluctuations [Fig. 4(b)] that are associated with the lower bulk modulii of this phase. The bulk modulii obtained from stress-strain calculations[35] are 190 GPa and 156 GPa for sc and the $I4_1/amd$ structures, respectively.

Vibrational free energy F_{vib} also contributes to the energetics at finite temperature, and, under some circumstances, can initialize phase transitions. One example is the martensitic transformation of Li from a 9R to a bcc structure.[36,37] F_{vib} can be obtained from thermodynamic integration and might be estimated from QHA if the anharmonicity is not highly pronounced in the system.[38] In the case of Ca, however, QHA might not be adequate for an accurate evaluation

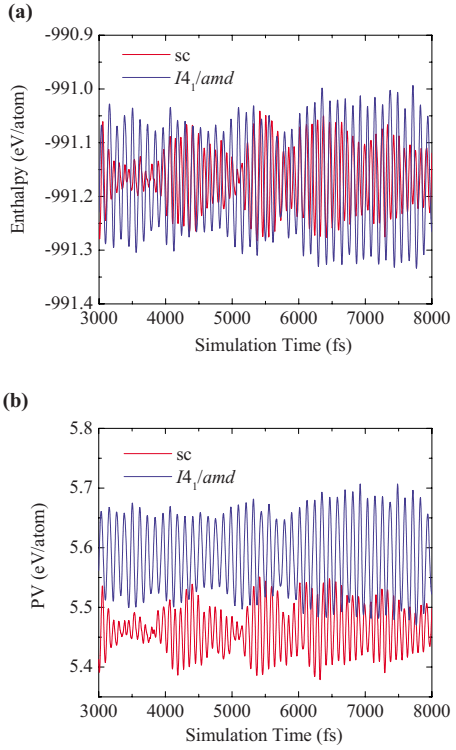

FIG. 4. (Color online) Calculated (a) enthalpy and (b) the energies from PV term of the sc and $I4_1/amd$ structures at 60 GPa and 300 K, as functions of simulation time from 3 to 8 ps.

of F_{vib}. Anharmonicity is of great importance in the structural stability of sc, which would be unstable in harmonic approximation (as indicated by imaginary phonons at 0 K).[12–14] The relative order of F_{vib} between the sc and $I4_1/amd$ structures can be qualitatively analyzed from the vDOS derived from the MD trajectories at 60 GPa and 300 K [Eq. (5)], which includes both harmonic and anharmonic vibrations. As shown in Fig. 5, the vDOS of the sc and $I4_1/amd$ structures are significantly different, especially in the frequency range below 250 cm^{-1}. The vDOS of sc is weighted much more heavily in the low-frequency acoustic range with a prominent peak arising around 50 cm^{-1}. Over the temperature range considered, the free energy arising from low-frequency vibrations are more effective in stabilizing the structure than are high-frequency vibrations.[39] The

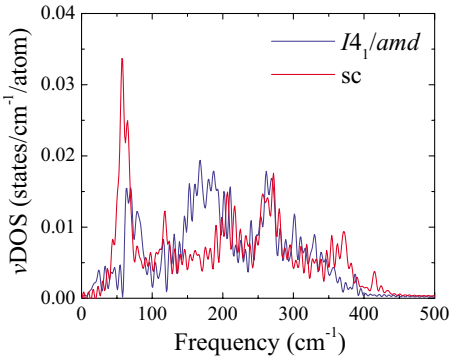

FIG. 5. (Color online) Calculated vDOS for the sc and $I4_1/amd$ structures at 60 GPa and 300 K.

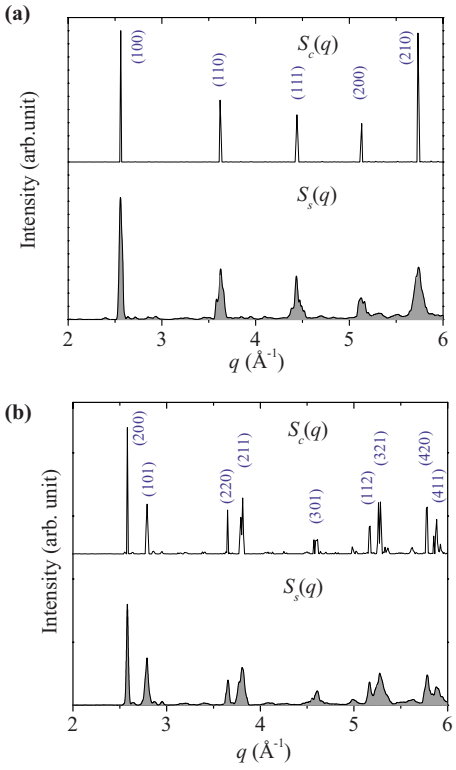

FIG. 6. (Color online) Calculated coherent structure factor $S_c(\vec{q})$ and static structure factor $S_s(\vec{q})$ for (a) the sc structure and (b) the $I4_1/amd$ structure at 60 GPa and 300 K.

enhanced weight of vDOS at low frequencies, therefore, results in a lower integrated F_{vib} in the sc structure. Using the vDOS in Fig. 5, the estimated F_{vib} for sc and $I4_1/amd$ structures at 60 GPa and 300 K from QHA are −0.014 eV/atom and −0.0096 eV/atom, respectively. These values of F_{vib}, albeit not quantitatively accurate as noted above, can however help to provide an estimate of the energy order for F_{vib}. These estimates can be combined with those obtained for the enthalpies to yield approximate Gibbs free energies. The result is that the $I4_1/amd$ is calculated to be slightly more stable at 300 K than the sc structure. If one employs a quasiharmonic calculation, which could be a poor approximation for Ca, one obtains a Gibbs free energy difference of 0.0006 eV with the $I4_1/amd$ phase being just marginally more stable. The observation that the enthalpy difference between $I4_1/amd$ and sc is much less at 300 K than at 0 K also indicates that the sc structure is becoming more stable with increasing temperature.

At 0 K, the sc is not a favorable structure by having both a higher enthalpy and distinct structural instability. The analysis above, however, shows that the sc structure becomes more energetically favorable and accessible at finite temperature. To examine the structural stability of sc structure at finite temperature, the coherent structure factor $S_c(\vec{q})$ was derived from the MD trajectory at 60 GPa and 300 K [Eq. (10)] and is displayed in Fig. 6(a). The first five Bragg peaks are located at 2.5609, 3.6214, 4.4317, 5.1219, and 5.7321 Å^{-1}, which are clearly associated with a sc lattice with an estimated lattice dimension of a=2.4535 Å. The sc structure remains stable and does not transform to any other

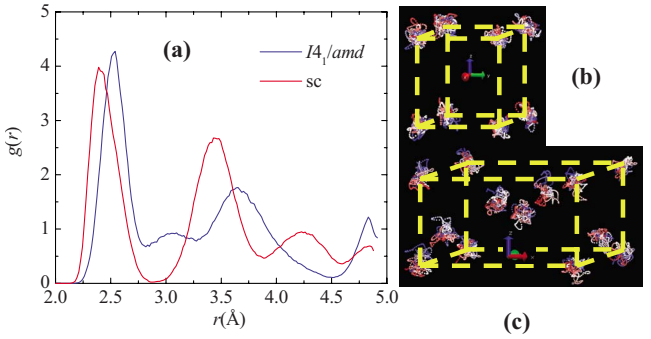

FIG. 7. (Color online) (a) Calculated radial distribution function obtained from the MD trajectories for the sc and the $I4_1/amd$ structures, at 60 GPa and 300 K. Calculated thermal trajectories sampled from MD calculations for (b) the sc structure and (c) the $I4_1/amd$ structure, at 60 GPa and 300 K. The trajectories are colored by the simulation time from beginning (blue) to end (red).

structures, at least during the simulation time. On the other hand, all Bragg peaks (except the very first one) have slight splitting. With the 64-atom supercell calculation, the splitting in the third peak is the largest and reaches about 0.02 Å^{-1}, while others are around 0.01 Å^{-1}. We note that the precise amount of splitting could be dependent on the simulation system size. Nevertheless, the peak splitting, albeit minor, indicates that at room temperature, the sc structure distorts slightly from the ideal sc lattice. In comparison with the sc structure, the $S_c(\vec{q})$ of the $I4_1/amd$ structure at same pressure and temperature reveals larger distortions [Fig. 6(b)]. The first nine most prominent Bragg peaks can be identified with a $I4_1/amd$ symmetry. Using the positions of the first two peaks, (200) and (101), a tetragonal unit cell is identified with a=4.689 Å and c=2.539 Å. All Bragg peaks except the first and third ones have notable broadening with the magnitude up to about 0.2 Å^{-1}. Although still keeping the basic lattice, the $I4_1/amd$ structure shows some indications of static disorder that is most likely related to it being less stable than sc at 300 K. It should be noted that the theoretical calculations estimate the heights of the reflections peaks using the tabulated atomic scattering form factors. The experimentally observed heights of XRD reflect a multiple of instrumental factors such as resolution of apparatus, and therefore cannot be exactly reproduced by theory. Apart from the Bragg reflections, the static structure factor $S_s(\vec{q})$, which captures instantaneous information of thermal motions, has also been calculated for the two structures [Figs. 6(a) and 6(b)]. Clearly, both $S_s(\vec{q})$ contain fairly broad peaks at the Bragg reflections, indicating large magnitudes of thermal motions in both structures.

Figure 7(a) shows the radial distribution function of Ca from the MD trajectories for the sc and $I4_1/amd$ structures at 60 GPa and 300 K. Although both structures have large thermal vibrations, the two structures are significantly different with essentially no overlap occurring. The calculated ensemble average of atomic displacements in the $I4_1/amd$ structure are weighted slightly more heavily in the larger magnitude range, which is associated with higher mobility of Ca atoms. A quantitative estimate of the magnitude of thermal motions is described by the isotropic thermal displace-

ment factors U_{iso}. In the present study, the calculated U_{iso} at 60 GPa and 300 K for the sc structure is 0.021 Å^2, while the value for the $I4_1/amd$ structure is slightly larger, 0.025 Å^2. Figures 7(b) and 7(c) display the MD trajectories sampled from MD calculations for sc and $I4_1/amd$ structures, respectively, colored (online only) by the simulation time from beginning (blue) to end (red). It can be seen that, although both trajectories have fairly large thermal motions, the vibrations are still centered on the symmetry sites for each structure. This observation suggests that the basic lattice of sc is stable and remains fixed within its thermal vibrations as seen in the diffraction simulation shown in Fig. 6(a). On the other hand, for the $I4_1/amd$ structure, larger thermal motions result in significant diffuse scattering and broadening of its Bragg peaks as seen in Fig. 6(b) which appears to indicate the onset of instability at 300 K.

The analysis of structure factors and thermal trajectories provides important insight into the relative stability of competing phases of Ca. In particular, although both have large thermal vibrations, the sc and $I4_1/amd$ structures are still distinguishable structures at room temperature. The peaks in $S_s(\vec{q})$ are broad but not broad enough to smear out the (tetragonal) peak splitting in the $I4_1/amd$ structure. The magnitudes of thermal motions are large but not large enough to indicate a structural interchange between the sc and $I4_1/amd$ structures. In order to accommodate the tetragonal splitting of the $I4_1/amd$ structure, the first peak (100) in the average cubic structure would have to be broadened to more than 0.5° in 2θ. This is also the case for other previously suggested *Cmcm* and *Pnma* structures of Ca. The diffraction patterns for these structures are even distinctly more different from that of the sc structure. This observation does not therefore provide support for a previous suggestion[17] that, at room temperature, the observed sc phase is an average structure of several competing structures although it is possible that energetically very close structures not yet considered could be contributing.

IV. CONCLUSIONS

In this study, an examination of the stability of the sc structure of Ca at 300 K in comparison with the recently predicted most stable low temperature $I4_1/amd$ structure was performed. This included a detailed examination of the electronic energy contributions determining the stability of these phases. It was found that the main difference between the two structures at $T=0$ and 60 GPa, for example, originated in long-range Coulomb interactions. The dynamical and thermodynamical stability of both sc and $I4_1/amd$ structures at room temperature was examined via first-principles MD simulations employing a *NPT* ensemble on a 64-atom supercell. These simulations provide a plausible support for and a basis to explain the dynamical stability of sc Ca at 300 K. Moreover, while at 60 GPa and $T=0$ the $I4_1/amd$ structure is stabilized with respect to the sc phase by an enthalpy difference of 0.076 eV/atom, at room temperature the enthalpies of the two structures become very close. The analysis of dynamical and structural properties suggests that sc Ca is not an average structure consisting of the lowest enthalpy $I4_1/amd$ and sc Ca but does not completely rule out the possibility that sc Ca at 300 K may be a mixture of other structures with very close energies or configurations.

Note added. Recently, there was a report[40] for the structure of Ca III at room temperature that finds a slightly distorted sc form with cell angle deviations from 90° to 89.9°.

ACKNOWLEDGMENTS

R.M. has been supported by the Slovak Research and Development Agency under Contracts No. APVV-0442-07 and No. VVCE-0058-07 and by the Vega Project No. 1/0096/08.

[1] H. Fujihisa, Y. Nakamoto, K. Shimizu, T. Yabuuchi, and Y. Gotoh, Phys. Rev. Lett. **101**, 095503 (2008).
[2] T. Yabuuchi, Y. Nakamoto, K. Shimizu, and T. Kikegawa, J. Phys. Soc. Jpn. **74**, 2391 (2005).
[3] Q. F. Gu, G. Krauss, Y. Grin, and W. Steurer, Phys. Rev. B **79**, 134121 (2009).
[4] R. Ahuja, O. Eriksson, J. M. Wills, and B. Johansson, Phys. Rev. Lett. **75**, 3473 (1995).
[5] H. Olijnyk and W. B. Holzapfel, Phys. Lett. **100A**, 191 (1984).
[6] T. Ishikawa, A. Ichikawa, H. Nagara, M. Geshi, K. Kusakabe, and N. Suzuki, Phys. Rev. B **77**, 020101(R) (2008).
[7] R. Martoňák, A. Laio, and M. Parrinello, Phys. Rev. Lett. **90**, 075503 (2003).
[8] Y. Yao, J. S. Tse, Z. Song, D. D. Klug, J. Sun, and Y. Le Page, Phys. Rev. B **78**, 054506 (2008).
[9] T. Ishikawa, H. Nagara, N. Suzuki, T. Tsuchiya, and J. Tsuchiya, Phys. Rev. B **81**, 092104 (2010).
[10] Y. Nakamoto, M. Sakata, K. Shimizu, H. Fujihisa, T. Matsuoka, Y. Ohishi, and T. Kikegawa, Phys. Rev. B **81**, 140106(R) (2010).
[11] S. Arapan, H.-K. Mao, and R. Ahuja, Proc. Natl. Acad. Sci. U.S.A. **105**, 20627 (2008).
[12] G. Gao, Y. Xie, T. Cui, Y. Ma, L. Zhang, and G. Zou, Solid State Commun. **146**, 181 (2008).
[13] A. M. Teweldeberhan and S. A. Bonev, Phys. Rev. B **78**, 140101(R) (2008).
[14] I. Errea, M. Martinez-Canales, A. R. Oganov, and A. Bergara, High Press. Res. **28**, 443 (2008).
[15] Y. Yao, D. D. Klug, J. Sun, and R. Martoňák, Phys. Rev. Lett. **103**, 055503 (2009).
[16] A. R. Oganov, Y. Ma, Y. Xu, I. Errea, A. Bergara, and A. O. Lyakhov, Proc. Natl. Acad. Sci. U.S.A. **107**, 7646 (2010).
[17] Z. P. Yin, F. Gygi, and W. E. Pickett, Phys. Rev. B **80**, 184515 (2009).
[18] M. T. Yin and M. L. Cohen, Phys. Rev. B **26**, 5668 (1982).
[19] M. C. Payne, M. P. Teter, D. C. Allan, T. A. Arias, and J. D. Joannopoulos, Rev. Mod. Phys. **64**, 1045 (1992).
[20] W. Kohn and L. J. Sham, Phys. Rev. **140**, A1133 (1965).
[21] A. A. Maradudin, E. W. Montroll, G. H. Weiss, and I. P. Ipatpva, *Theory of Lattice Dynamics in the Harmonic Approximation*,

2nd ed. (Academic, New York, 1971).
[22] M. L. Klein, in *Molecular Dynamics Simulation of Statistical Mechanical Systems*, edited by G. Ciccotti and W. G. Hoover (North Holland, Amsterdam, 1986), p. 426.
[23] *International Tables for Crystallography*, Vol. B, edited by U. Shmueli, 3rd ed. (Springer, New York, 2008).
[24] J. M. Soler, E. Artacho, J. D. Gale, A. García, J. Junquera, P. Ordejón, and D. Sánchez-Portal, J. Phys.: Condens. Matter **14**, 2745 (2002).
[25] G. Kresse and D. Joubert, Phys. Rev. B **59**, 1758 (1999).
[26] G. Kresse and J. Hafner, Phys. Rev. B **47**, 558 (1993).
[27] J. P. Perdew, K. Burke, and M. Ernzerhof, Phys. Rev. Lett. **77**, 3865 (1996).
[28] J. Junquera, Ó. Paz, D. Sánchez-Portal, and E. Artacho, Phys. Rev. B **64**, 235111 (2001).
[29] H. J. Monkhorst and J. D. Pack, Phys. Rev. B **13**, 5188 (1976).
[30] A. Becke and K. E. Edgecombe, J. Chem. Phys. **92**, 5397 (1990).
[31] S. Nosé, J. Chem. Phys. **81**, 511 (1984).
[32] M. Parrinello and A. Rahman, J. Appl. Phys. **52**, 7182 (1981).
[33] M. Alatalo, P. Asoka-Kumar, V. J. Gogh, B. Nielsen, K. G. Lynn, A. C. Kruseman, A. van Veen, T. Korhonen, and M. J. Puska, J. Phys. Chem. Solids **59**, 55 (1998).
[34] R. Ahuja and B. Johansson, J. Appl. Phys. **89**, 2547 (2001).
[35] Y. Le Page and J. R. Rodgers, J. Appl. Crystallogr. **38**, 697 (2005).
[36] H. G. Smith, Phys. Rev. Lett. **58**, 1228 (1987).
[37] A. Y. Liu, A. A. Quong, J. K. Freericks, E. J. Nicol, and E. C. Jones, Phys. Rev. B **59**, 4028 (1999).
[38] J. Xie, S. de Gironcoli, S. Baroni, and M. Scheffler, Phys. Rev. B **59**, 965 (1999).
[39] Y. Yao, J. S. Tse, K. Tanaka, F. Marsiglio, and Y. Ma, Phys. Rev. B **79**, 054524 (2009).
[40] W. L. Mao, L. Wang, Y. Ding, W. Yang, W. Liu, D. Y. Kim, W. Luo, R. Ahuja, Y. Meng, S. Sinogeikin, J. Shu, and H.-k. Mao, Proc. Natl. Acad. Sci. U.S.A. **107**, 9965 (2010).